# **Aqueous Solvation Dynamics at Metal Oxide Surfaces**

Erwin Portuondo-Campa,† Andreas Tortschanoff,\*,† Frank van Mourik,† Jacques-Edouard Moser,‡ Andreas Kornherr,§ and Majed Chergui\*,†

Laboratoire de Spectroscopie Ultrarapide, ISIC, Ecole Polytechnique Fédérale de Lausanne, CH-1015 Lausanne, Switzerland, Laboratoire de Photonique et Interfaces, ISIC, Ecole Polytechnique Fédérale de Lausanne, CH-1015 Lausanne, Switzerland, and Institute of Physical Chemistry, University of Vienna, Währingerstrasse 42, A-1090 Wien, Austria

Received: November 8, 2005; In Final Form: February 28, 2006

Broadband transient absorption (TA) spectroscopy, three-pulse photon echo peak shift (3PEPS), and anisotropy decay measurements were used to study the solvation dynamics in bulk water and interfacial water at  $ZrO_2$  surfaces, using Eosin Y as a probe. The 3PEPS results show a multiexponential behavior with two subpicosecond components that are similar in bulk and interfacial water, while a third component of several picoseconds is significantly lengthened at the interface. The bandwidth correlation function from TA spectra exhibits the same behavior, and the TA spectra are well reproduced using the doorway-window picture with the time constants from PEPS. Our results suggest that interfacial water is restricted to a thickness of less than 5 Å. Also the high-frequency collective dynamics of water does not seem to be affected by the interface. On the other hand, the increase of the third component may point to a slowing down of diffusional motion at the interface, although other effects, may play a role, which are discussed.

#### Introduction

The dynamics of molecular motion in bulk water occur on a very fast time scale, and the results from different femtosecond time-resolved optical experiments based on optical-Kerr effect (OKE),<sup>1,2</sup> hole burning,<sup>3</sup> photon-echo techniques,<sup>4-9</sup> pumpprobe spectroscopy, 10 and fluorescence up-conversion, 11,12 in addition to frequency-domain Raman and infrared studies, indicate a complex picture of multiexponential dynamics, which is supported by extensive theoretical and computational work. The underlying processes include diffusive and hindered vibrational motions of water molecules and hindered translational motions of the hydrogen-bonded network, strongly influenced by the hydrogen bond forming and breaking, and the long-range order, which is present in bulk water. Studies of polar solvation dynamics in water revealed a nonexponential behavior on a subpicosecond time scale, faster than in most other solvents, with an ultrafast Gaussian initial component due to inertial motion and two exponential decays. 11,13 More recently, it was also argued that there is a slower component due to diffusive rotational motions of individual water molecules.<sup>7</sup>

Many important reactions and fundamental processes take place at interfaces, membranes, and restricted environments, where the properties of the solvents change in a drastic manner. Numerous studies<sup>14–18</sup> show that the structure of water at interfaces is different from its structure in the bulk, and depends strongly on properties of the interfaces. An "icelike" structure was invoked for both hydrophobic<sup>16</sup> and hydrophilic<sup>14,15</sup> surfaces, but recent investigations using surface vibrational sum

frequency spectroscopy indicate a rather liquidlike character.<sup>19</sup> Neutron diffraction studies of confined water in various types of porous silica<sup>20,21</sup> have been interpreted as indications that, at room temperature, water in the vicinity of hydrophilic surfaces is in a state equivalent to that of supercooled bulk water. Because of these structural differences, we expect the *dynamics* of water close to interfaces to be different from that of the bulk. Much less is known about the microscopic processes underlying solvation and solvent reorientation close to surfaces, which are of great importance for our fundamental understanding of surface reactions and biological functions.

Many experimental and theoretical studies of solvation dynamics of water in complex environments<sup>22</sup> point to different solvent behavior. In time-resolved experiments of aqueous solvation dynamics at interfaces, femtosecond fluorescence upconversion experiments of tryptophan residues at the surface of proteins<sup>23-25</sup> show dynamics that are slower than those in bulk water by an order of magnitude, within a layer of biological water of less than 8 Å thickness. Similar studies<sup>7,26</sup> with dyes attached to membranes indicate a substantial disruption of the hydrogen-bonded network, while the diffusive single molecule reorientation of water seems to contribute to solvation at the interface in the same manner as it does in the bulk. Recently, ultrafast electron diffraction experiments showed that the time scale for the breakage of long-range order of the interfacial layer is an order of magnitude longer than that for breaking hydrogen bonds in bulk liquid water.<sup>27</sup>

While much of the interest on interfacial water structure and dynamics focuses on biological systems, the dynamical properties of water at crystalline solid surfaces are also of high scientific and practical interest. For example Ti is the most widely used metal in medical applications and its biocompatibility is closely related to the chemistry of TiO<sub>2</sub>/water interfaces. In addition, TiO<sub>2</sub> is used in solar cells that are based on metal coordination compounds at the interface in an electrolyte.<sup>28</sup>

<sup>\*</sup>To whom correspondence should be addressed: Andreas.Tortschanoff@epfl.ch, Majed.Chergui@epfl.ch.

 $<sup>^\</sup>dagger$  Laboratoire de Spectroscopie Ultrarapide, ISIC, Ecole Polytechnique Fédérale de Lausanne.

<sup>&</sup>lt;sup>‡</sup> Laboratoire de Photonique et Interfaces, ISIC, Ecole Polytechnique Fédérale de Lausanne.

<sup>§</sup> Institute of Physical Chemistry, University of Vienna.

In previous studies, 29,30 a coumarin (C343) dye was used to probe the solvation dynamics of water at the surface of ZrO<sub>2</sub> nanoparticles via femtosecond-fluorescence up-conversion. A faster overall response of the interfacial water as compared to bulk water was reported, which the authors related either to a prealignment of the water molecules at the ZrO<sub>2</sub> surfaces or, alternatively, to a disruption of the hydrogen bond network at the surface, making the water molecules looser. A similar upconversion-study in our group<sup>31</sup> (with improved temporal and spectral resolution) confirmed these results. However, these studies raise several questions: Upon adsorption to the surface, the absorption band of coumarin 343 shows a large red shift, indicative of covalent binding of the chromophore. Due to this large shift, the excitation conditions at 400 nm are quite far above resonance, putting more internal energy in the adsorbed dye, so that the direct comparison to the results of bulk water is questionable.<sup>29</sup> Also a recent molecular dynamics study of this system indicated that, very generally, aqueous solvation is different for the deprotonated and the neutral form of the dye, which predominantly adsorbs at the surface.<sup>32</sup> Therefore, it is not clear whether the reported dynamics really bears the signature of the interfacial water or is dominated by intramolcular relaxation or adsorbate-surface interaction. Still, faster dynamics, as compared to the bulk, were also reported for the IR144 dye at the surface of SiO<sub>2</sub> particles in two different solvents, using time-resolved second harmonic generation. 14,15,33

In this contribution, we apply the same basic idea as in refs 29-31, namely, to use dyes, attached to the surface of ZrO<sub>2</sub> nanoparticles, as probes of the ultrafast solvation dynamics of the interfacial water. But here, we extend the range of techniques to probe the interface, by performing transient absorption and photon echo experiments, in addition to fluorescence upconversion. ZrO<sub>2</sub> is used as a model system, because of the high efficiency of electron injection into TiO2 34 upon optical excitation of dyes attached to its surface. ZrO2 has a higher band gap than TiO2, which prevents quenching via electron injection. To overcome the problem of the strong shift of the absorption spectrum of coumarin upon adsorption, in the present study, we used eosin Y, which is known to electrostatically bind to the surface<sup>35</sup> and has the advantage that the optical properties do not change significantly upon adsorption. Measurements of eosin attached to the surface are compared to experiments of eosin in bulk water.

### **Solvation Dynamics**

In typical solvation dynamics studies, a perturbation is introduced in the system, e.g., in the form of a spontaneous change of dipole moment in the chromophore, and the relaxation of the solvent molecules to a new equilibrium is probed via the time-resolved fluorescence Stokes shift (TRSS) by means of fluorescence up-conversion<sup>12</sup> or pump-supercontinuum—probe experiments.<sup>36</sup> The experimental and theoretical backgrounds of solvation dynamics in liquids are well established, and the dynamics is usually quantitatively characterized by the normalized energy-gap function S(t).

$$S(t) = \frac{\Delta E(t) - \Delta E(\infty)}{\Delta E(0) - \Delta E(\infty)} \tag{1}$$

 $\Delta E(t)$  is the gap between the chromophore electronic ground and excited state at time t and can readily be obtained from the maximum of the time-resolved fluorescence spectra.

According to the Onsager regression hypothesis, for small perturbations, the relaxation of the excited solute energy gap

back to equilibrium behaves identically to the relaxation dynamics of the unperturbed solute upon natural fluctuations of the gap away from equilibrium.<sup>37</sup> Within the limits of this linear response approximation, S(t) is identical to the correlation function M(t) of equilibrium fluctuations of the optical transition frequency  $\delta \omega_{ve}$ 

$$S(t) = M(t) = \frac{\langle \delta \omega_{\text{ge}}(t) \delta \omega_{\text{ge}}(0) \rangle}{\langle \delta \omega_{\text{ge}}^2 \rangle}$$
 (2)

Even if this approximation is to be used with some caution, especially if there are simultaneous changes in size and shape of the solute,  $^{38,39}$  it has proven to be extremely valuable in many studies of polar solvation and the goal of optical experiments usually is to find accurate expressions for M(t).

Further, M(t) is also equivalent to the bandwidth correlation function W(t), which is measured in hole burning and pump—probe experiments

$$W(t) = \left(\frac{\sigma(t)^2 - \sigma(\infty)^2}{\sigma(0)^2 - \sigma(\infty)^2}\right)^{1/2} \tag{3}$$

where  $\sigma(t)$  is the bandwidth of the spectrum (or hole). Again this relation is based on the assumption that the same fluctuation processes, which take place in the bath at equilibrium, are responsible for the broadening of the spectrum and for the relaxation toward equilibrium after a perturbation. We can observe this process in time by creating a hole in the absorption spectrum and following its broadening. Note that whereas with the TRSS measurements one observes the relaxation times via the fluorescence from the excited state, in hole burning and pump-probe measurements both the band broadening in the ground state hole and in the excited state population can be seen. These are similar only within the limits of linear response theory, and differences between spectral shift and broadening functions were previously observed, 40,41 where the time correlation function of the solvent relaxation observed from the spectral bandwidth was slower than that from the time-dependent shift of the fluorescence maximum. It seems that the energy relaxation is largely controlled by the rapid rotational diffusion of solvent molecules, whereas the slower, collective, translational diffusion is mainly responsible for the relaxation process of the spectral width.40

Linear response theory is the basis for most of the work on solvation and solvation dynamics and has shown to be extremely useful in previous investigations. Limits of its applicability were discussed, <sup>38,39,42,43</sup> and one might argue whether it should hold for molecules at the surface. In this paper, we rely on this approximation, in part because it is difficult to go beyond it for analytic descriptions of optical signals and also because recent molecular dynamic studies of tryptophan in a complex protein environment<sup>44</sup> and of coumarin at a ZrO<sub>2</sub> surface<sup>32</sup> strongly suggest the validity of linear response for these systems. However, we are planning molecular dynamics simulations of eosin at the TiO<sub>2</sub>—water interface to elucidate this and related questions.

It was shown<sup>7,45,46</sup> that a good estimate for the decay of M(t) can be obtained from three-pulse photon echo peak shift (3PEPS) measurements. Here the sample is irradiated by a sequence of three identical resonant pulses and the time integrated photon echo signal is recorded as a function of both interpulse delays,  $t_{12}$  and  $t_{23}$ .  $t_{12}$  and  $t_{23}$  are also termed coherence and population period, respectively, because during  $t_{12}$  the chromophore resides in an optical coherence, whereas during

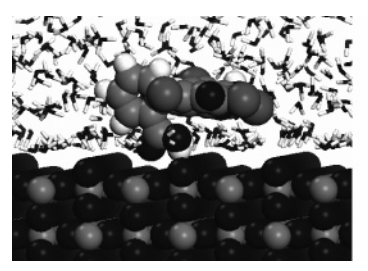


Figure 1. (left) Eosin adsorption on a stoichiometric rutile TiO<sub>2</sub> (110) surface. The surface and the eosin molecule are visualized by balls; the water molecules are indicated by lines (black, O; dark gray, Br; gray, C or Ti; white, H). (right) Structure of eosin Y.

 $t_{23}$  we observe the population grating imprinted in the sample. In the 3PEPS experiment for each  $t_{23}$  the time-integrated signal is determined as a function of  $t_{12}$ . The  $t_{12}$  corresponding to the maximum signal is termed the echo peak shift.

In the Bloch limit, the magnitude of the peak shift is a measure of the ratio between inhomogeneous and homogeneous contributions to the electronic line broadening dynamics.<sup>47</sup> In general, in condensed phase systems there is no distinct separation of time scales. It was shown that in this case the decay of the echo peak shift follows the decay of M(t) very accurately, except for the very early times, where an inherent discrepancy exists between the correlation function and the echo peak shift.47,48

According to dielectric continuum theory, the decay observed in TRSS measurements reveals the dielectric relaxation via the longitudinal relaxation time  $\tau_{\rm L}$ .<sup>49,50</sup> For the solvation of a dipole,  $\tau_{\rm L}$  is connected to the transverse (Debye) relaxation via

$$\tau_{\rm L} = \frac{2\epsilon_{\infty} + 1}{2\epsilon_0 + 1} \tau_{\rm D} \tag{4}$$

where  $\epsilon_{\infty}$  and  $\epsilon_0$  are the static and optical dielectric constant, respectively.<sup>49</sup> In a first approximation, water is often described with a single Debye relaxation time of  $\tau_D = 8.2$  ps, which would predict decay times  $\tau_L$  of less than 1 ps.

## **Experimental Section**

Sample Preparation. The chromophore used in these experiments was eosin Y (Figure 1, right), which was purified by column chromatography and repeated recrystallization of its protonated form in water.<sup>35</sup>

For bulk solvation a  $4 \times 10^{-5}$  M solution of eosin was prepared in 0.3 M acetate buffer, pH 4.0. For interfacial water dynamics, eosin was added to a colloidal suspension of ZrO2 particles (Alfa Aesar) with a diameter of 5-10 nm, in aqueous acetic acid diluted to 0.3 M, pH 4.0. The nanoparticles concentration was estimated to be  $1 \times 10^{-4}$  M. Eosin was added in a concentration of  $4 \times 10^{-5}$  M. Thus, less than one dye molecule per nanoparticle is present in the solution to avoid dye-dye interactions and aggregate formation on the ZrO2 surface. At this pH, eosin is singly charged and effectively adsorbs on the ZrO<sub>2</sub> surface.<sup>35</sup> For the photon echo studies, 10fold higher concentrations of nanoparticles and dye were used.

Pump Supercontinuum Probe (PSCP). The amplified 1 kHz, 800 nm radiation of a mode-locked Ti:sapphire laser (Spectra Physics) was split in two beams. The first was used to generate the pump pulse in a home-built noncollinear optical parametric amplifier (NOPA)<sup>51</sup> providing sub-40-fs pulses centered at 532 nm. The pump pulses were focused on the sample in a spot of 250  $\mu$ m diameter. The intensity was adjusted with a neutral density filter to 50 nJ per pulse. The second 800 nm beam was used to generate supercontinuum light in a sapphire window. The white light, ranging from 420 to 800 nm, was directed and focused on the sample with parabolic mirrors. The measured size of the probe focus was 160  $\mu$ m and the total energy per pulse was 2 nJ. A syringe pump kept the sample flowing in a 0.3 mm cell, at a rate that ensured complete renewal of the exposed volume between laser shots. The transmitted probe beam was recorded with a diode array, and the transient absorption signal  $\Delta OD$  was calculated. The chirp of the white light probe beam was measured using the cross-phase modulation signal of pure water, and the data were corrected accordingly.

Three-Pulse Photon-Echo Peak Shift. For the 3PEPS measurements 50-fs pulses of 525 nm central wavelength were generated in an optical parametric amplifier pumped by an amplified Ti:sapphire laser system with 250 kHz repetition rate (Coherent RegA-9050). The beam was split into three equal beams (1, 2, and 3) which, after passing computer-controlled delay stages, were recombined in a triangular geometry and focused on the sample using a singlet quartz lens with a 15 cm focal length. The diameter of the focal spot at the sample was about 150  $\mu$ m, and the pulse energy ca. 8 nJ. Beams 1 and 2 passed a high-precision piezo flexure stage while beam 3 could be individually delayed with a 0.1  $\mu$ m resolution motorized translation stage. The sample was pumped through a 0.1 mm flow cell, which in addition was translated perpendicular to the beam direction, to avoid deposition of ZrO<sub>2</sub> in the focal spot

The four-wave mixing signal generated in the sample in the phase-matching directions was detected by photodiodes and processed with an eight-channel fast sample and hold AD board (Becker&Hickl, SHM-180) allowing single shot detection. For the experiments the signal was simultaneously detected in the two directions  $-k_1 + k_2 + k_3$  and  $-k_2 + k_1 + k_3$ , where  $k_1, k_2$ , and  $k_3$  are the wavevectors of pulses 1, 2, and 3, respectively. For exact time zero calibration, we further measured the third conjugate direction  $-k_3 + k_1 + k_2$  and verified that at the position of the zero time delay the three pulse echoes exactly overlapped with the two pulse echoes  $(-k_1 + 2k_2, -k_2 + 2k_1)$ . A 3PEPS scan consists for each population time  $T_{23}$  of one scan of delay stage 1 and one of stage 2 to get the two conjugate photon-echo signals. These curves were fitted to Gaussians to find the maximum. The photon-echo peak shift is half the distance between the maxima in the  $t_{12}$  delays.

Anisotropy Decay Measurements. To estimate the average fraction of effectively bound eosin Y molecules, we measured the anisotropy decay. The anisotropy is defined as  $r(t) = (I_{||} - I_{||})$  $I_{\perp}$ )/ $(I_{\parallel} + 2I_{\perp})$ , where  $I_{\parallel}$  and  $I_{\perp}$  are the pump-probe signals measured for parallel and perpendicular probe polarization, with respect to the polarization of the pump beam, respectively. These measurements were performed with the same setup as the photon echo, using only two of the three pulses and adjusting the relative intensity to about 10:1. High-quality film polarizers were used to ensure that the pump beam was vertically polarized. The probe beam was polarized at 45° with respect to the pump and, after passing the sample, separated into its parallel and perpendicular components (with respect to the pump) by means of a polarizing cube beam splitter. The two components were simultaneously detected with two photodiodes, which were adjusted to equal signal with the pump beam blocked. By chopping the pump beam, we measured the difference of the transmitted signal with and without pump, i.e., the single color pump-probe signals.

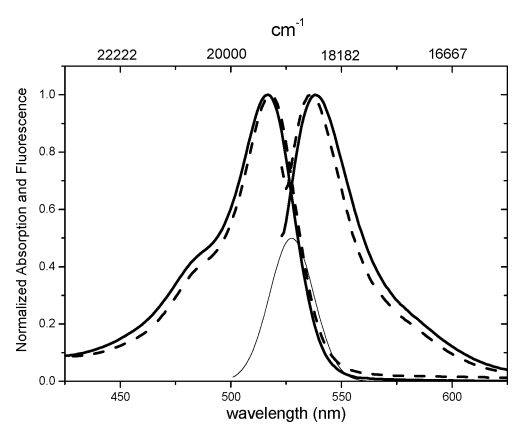


Figure 2. Absorption and emission spectra of eosin in bulk water (solid lines) and at the surface of ZrO<sub>2</sub> (dashed lines). The Gaussian curve indicates the spectrum of the pump pulse.

### **Experimental Results**

# Figure 2 shows the absorption and fluorescence spectra of eosin in bulk water and adsorbed at the ZrO<sub>2</sub> surface. Semiempirical quantum mechanical calculations show that the transition at 520 nm is of $\pi$ - $\pi$ \* character, with the HOMO distributed on the xanthene fused ring part.<sup>35</sup> Optimization of the molecule geometry indicates that the benzoic ring moiety is rotated perpendicular to the xanthene plane, thus making the coupling of the

Steady-State Spectra and Time-Resolved Anisotropy.

carboxylic group with the chromophore unlikely. The fluorescence spectrum of eosin is the mirror image of the absorption indicating similar ground- and excited-state geometries. There is only a small red shift of about 2 nm in the absorption

spectrum upon adsorption, which is a good indication that the chromophore part of the dye is not strongly affected by adsorption. In fact, it binds mainly via the charged carboxylic group, attached to the phenyl ring (cf. Figure 1), which has an orthogonal configuration with regard to the transition dipole moment of the electronic transition (as also indicated by semiempirical quantum mechanical calculations<sup>35</sup>). The large chromophore lies parallel to the surface at a distance of  $\sim 5$  Å. Also the fluorescence spectra of the free and adsorbed dye look very similar. The Stokes shift of adsorbed eosin is somewhat smaller than that for free eosin: 650 and 775 cm<sup>-1</sup>, respectively. There is no signature of aggregate formation on the surface, which would be observed at significantly higher concentrations.<sup>35</sup> At pH 4, the surface of the ZrO<sub>2</sub> particles is positively charged. The carboxylic group of eosin Y, with a p $K_a$  of 3.4,<sup>52</sup> is deprotonated and constitutes a negative charge that electrostatically binds the dye to the surface.<sup>35</sup>

To make sure that the dye is actually attached to the surface of the ZrO<sub>2</sub> nanoparticles, we measured the rotational correlation time by time-resolved anisotropy r(t). The result is shown in Figure 3. The time-resolved anisotropy of eosin in solution decays with a time constant of 160 ps, which corresponds to the rotational diffusion of eosin.<sup>53</sup> It is significantly faster than the value of 350 ps reported for the eosin Y dianion,<sup>54</sup> where strong solute-solvent hydrogen-bond formation plays an essential role in slowing down the reorientational process, indicating that strong and highly specific interactions to solvent water in the first layer play a minor role at our experimental conditions, where eosin is mainly singly charged.

In contrast, the decay of eosin adsorbed to the ZrO2 nanoparticles is much slower. The ZrO2 colloids have an average diameter of 5-10 nm, corresponding to a very slow rotational decay within tens of nanoseconds<sup>55</sup> and essentially constant on

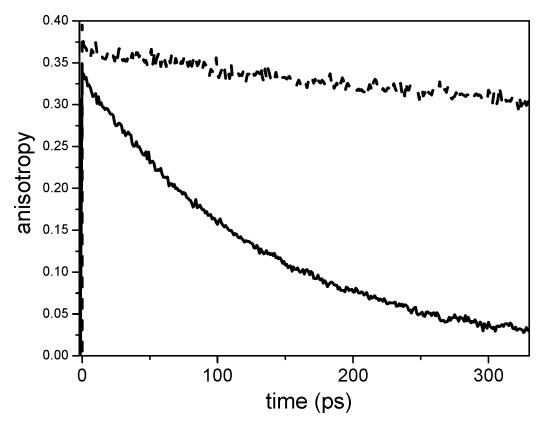


Figure 3. Anisotropy decay of eosin (dashed line, adsorbed on ZrO<sub>2</sub>; solid line, in water).

the time scale of these measurements. Assuming equilibrium between rigidly bound and completely free eosin, we find that at least 80% of the molecules are statically attached to the surface during the time scale of the experiment. More realistically close to 100% of the dye is bound and the anisotropy is reduced due to wobbling motions of the dye. In preliminary calculations eosin Y was found to adsorb to TiO2 with a binding energy of  $E_{\rm ads} \approx 140$  kJ/mol in a configuration as shown in Figure 1. Under the assumption of unhindered motion up to a maximum angle  $\alpha_c$ , we can estimate a cone angle of  $\alpha_c = 21^\circ$ for the motions of the chromophore at the surface.<sup>55</sup>

Finally, we performed the anisotropy measurements with freshly prepared solutions, right after adding the dye to the ZrO<sub>2</sub> colloidal suspension and after letting the solution equilibrate overnight. There was no difference, indicating that adsorption occurs very quickly.

Our anisotropy measurements indicate that the dye binds well to the surface and stays bound upon optical excitation. Probe molecule translation away from the surface, as discussed recently in theoretical studies for confined solvents,<sup>56</sup> can be excluded. Possible reorientations after excitation could play a role, but we do not expect major rearrangements because the chromophore part of the molecule, where the electronic excitation takes place, is decoupled from the carboxylic group, which is predominantly responsible for binding of the molecule to the surface. Also the static spectra do not strongly change upon

Photon Echo Peak Shift. The 3PEPS signals for eosin in bulk water and at the surface are shown in Figure 4. They are characterized by a sub-100-fs initial decay, followed by a longer one on the picosecond time scale.

The ultrafast component includes inertial contributions from librational motions of water molecules in the first hydration shells<sup>8</sup> but, as outlined above, the signal correctly reflects the decay of M(t) only for longer time scales and the first initial components of the PEPS signal are very sensitive to rapid intramolecular dephasing processes.<sup>47</sup> The curves were fitted to a three-exponential target function to extract the different time scales of solvation.

Table 1 shows the results of the fits. In some cases, the time constants were fixed to the results of refs 8 and 26. From the correlation values  $R^2$  (last column), we can nicely fit the data with these literature values (except the ultrafast component, which strongly depends on the pulse length). Letting all parameters free, we also find somewhat similar time constants and only a slight improvement in the quality of the fit.

It is interesting that for both eosin in water and eosin at the surface, we get the same characteristic decay time  $t_2$  of ca. 700

TABLE 1: Results from Three-Exponential Fits  $(A_1 \exp(-t/t_1) + A_2 \exp(-t/t_2) + A_3 \exp(-t/t_3) + y_0)$  of the Photon Echo Peak

	$A_1$	t <sub>1</sub> (fs)	$A_2$	$t_2$ (fs)	$A_3$	$t_3$ (fs)	$y_0$	$\chi^2$	$R^2$
H <sub>2</sub> O (ref 8)	$18.9 \pm 0.9$	$20.7 \pm 0.9$	$1.2 \pm 0.1$	400	$1.4 \pm 0.1$	2700	$0.67 \pm 0.03$	0.01528	0.99579
H <sub>2</sub> O (ref 26)	$18.4 \pm 0.8$	$21.8 \pm 0.9$	$1.9 \pm 0.1$	1000	$0.5 \pm 0.1$	7500	$0.63 \pm 0.04$	0.01551	0.99573
H <sub>2</sub> O free fit	$18.7 \pm 0.8$	$21 \pm 1$	$1.7 \pm 0.2$	$710 \pm 170$	$0.8 \pm 0.2$	$5800 \pm 2600$	$0.62 \pm 0.05$	0.01536	0.99602
H <sub>2</sub> O/ZrO <sub>2</sub> free fit	$13 \pm 1$	$16 \pm 2$	$1.1 \pm 0.4$	$700 \pm 400$	$0.6 \pm 0.3$	10000	$2.8 \pm 0.1$	0.11718	0.96177

<sup>&</sup>lt;sup>a</sup> The first two rows show fits to eosin in water with  $t_2$  and  $t_3$  values taken from refs 8 and 26.

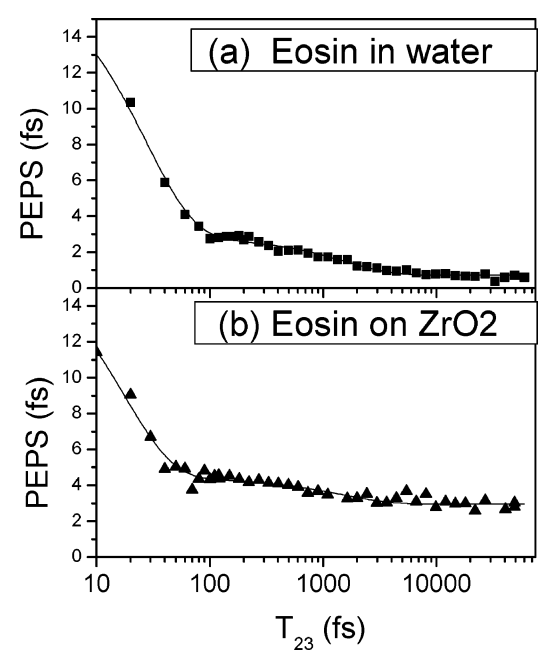


Figure 4. 3PEPS scans of eosin in water (a) and eosin at the surface of  $ZrO_2$  (b).

fs, indicating very similar dynamics of the water solvation. We further find a much slower time constant, which increases strongly for the case of adsorbed eosin, and whose physical meaning is still under debate.<sup>26</sup> However, there is a large uncertainty due to the rather strong noise in the long time tail of the measurements. In fact, for the experiments on bound eosin, this component was estimated from the decay at long delay times and then kept fixed in the three exponential fitting procedure.

The most striking difference between our measurements on eosin in bulk water and at the interface is the amplitude of the signal offset at long times (Figure 4). There is a significantly increased offset value for eosin bound to the surface compared to the free dye, which indicates residual inhomogeneity on time scales longer than the time scales of the experiment, i.e., > 100 ps. We think this reflects the very complicated and ill-defined local structure and distribution of binding configurations of the eosin molecule at the surface of ZrO<sub>2</sub> and possibly slow solute reorientation on nanosecond time scales.<sup>32</sup>

We should stress that fitting the curves to a three-exponential decay does not correspond to a specific underlying model or represents the actual processes occurring in water, but it is rather meant as a parametrization to quantify the time scales and to compare our results with similar experiments in the literature. Actually, recent OKE experiments on water indicated that the derivative of a stretched exponential decay might be most suitable to fit the slow relaxation of water.<sup>2</sup>

Since the goal of this investigation is the comparison of dynamics in bulk water with that at the interface, rather than an accurate description of aqueous solvation dynamics by a consistent model (such as, e.g., the detailed investigations of Lang et al.8 or Bürsing et al.,7 who used the Brownian oscillator

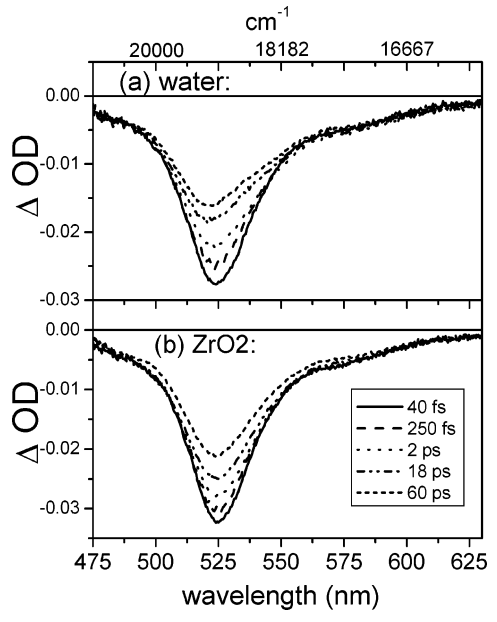


Figure 5. Transient spectra of eosin in water (a) and eosin on the surface of ZrO2 (b).

model), we will stay with the above phenomenological fitting and focus on the comparative features between bulk solvent and interface.

Pump-Probe Spectroscopy. Transient spectra at various delay times are shown in Figure 5. Within some tens of femtoseconds the spectra reach their final global shape. In the pulse overlap region and the first femtoseconds, there are rapidly changing features, which are due to remaining cross-phase modulation in water (not shown here). The broad negative band comes from ground-state bleaching and stimulated emission. On the blue side, we further have contributions from excitedstate absorption,<sup>57</sup> (not shown) which result in a small positive signal below 460 nm.

The analysis of the time traces taken at the maximum and at the red side of the transient spectra shows rising components in the stimulated emission at around 590 nm, an indication of the energy flow in the excited state due to vibrational and solvent-induced relaxation.<sup>57</sup> The decay of the transient signals at the maximum of the band can be fitted to a biexponential decay with times of ca. 0.2 and 7 ps, very similar for free eosin and eosin at the surface.

Spectra a and c of Figure 6 show normalized transient pumpprobe spectra of eosin in water and at the ZrO2 surface for different time delays, which demonstrate the broadening of the features and a weak blue shift of the maximum of the band with time. The broadening can be quantified by plotting the variance (i.e., the second moment of the signal in the region from 487 to 574 nm) as a function of time (Figure 7a).

The initial signals at very short delay times look identical, and due to selective excitation on the red edge of the absorption spectrum with the pulse centered at 532 nm (fwhm = 35 nm, cf. Figure 2), they show a pronounced narrowing due to hole

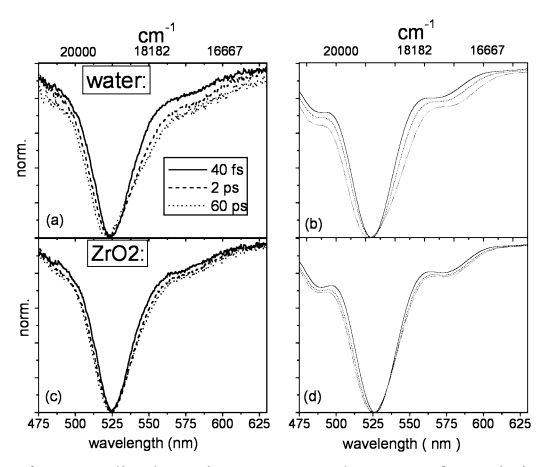


**Figure 6.** Normalized transient pump—probe spectra for eosin in water (a, b) and eosin bound to  $ZrO_2$  (c, d): left column, experimental data; right column, calculated curves (see text for details).

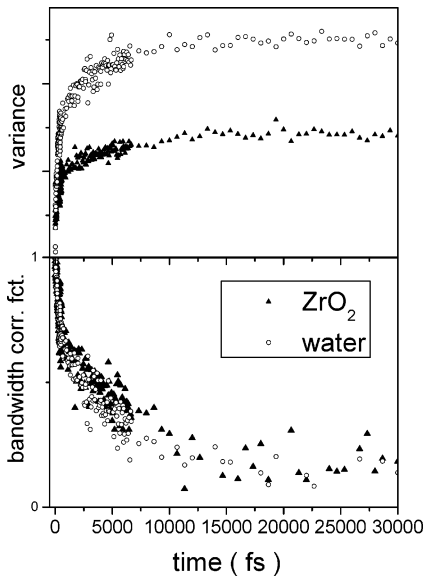
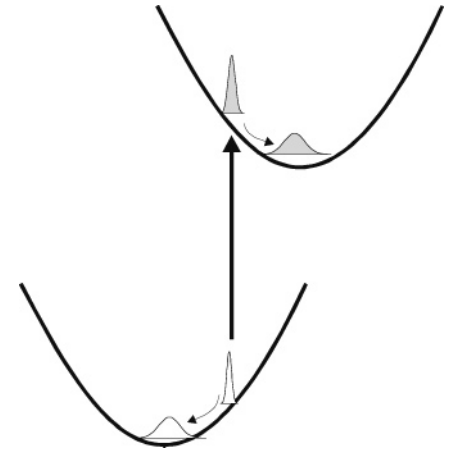


Figure 7. (a) "Variance" of the transient signal. (b) Bandwidth correlation function

burning. The initial full width at half-maximum is ca. 1300 cm<sup>-1</sup>. From the overlap of the laser with the absorption spectrum, however, we would expect an initial hole with a width of ca. 550 cm<sup>-1</sup>. Thus the transient signal we observe after 50 fs already includes substantial broadening, indicative of ultrafast initial relaxation processes. The subsequent broadening is related to slower solvation processes. It is significantly more pronounced in bulk water than at the interface.

## Analysis of the Data

In our experiment, the short pump pulse excites part of the molecules generating a population of "particles" in the first excited state and leaving a hole in the ground state. Particle and hole show dynamical evolution as they return to equilibrium<sup>58–60</sup> (cf. Figure 8). As indicated in Figure 8, there is a shift in the central energy of particle and hole as well as a temporal broadening and we expect a blue shift in the bleach signal, which results from the relaxation of the hole, and a red shift in the stimulated emission, reflecting the time-resolved Stokes shift due to relaxation in the excited state. Possible dynamics in the excited-state absorption bands strongly depend on the electronic potential of the final state.<sup>36</sup> The most important dynamics for both, particle and hole of our system, which has



**Figure 8.** Sketch of a pump—probe measurement: The potential curves represent the energy of the ground and excited state along some arbitrary solvation coordinate. The vertical arrow indicates excitation by a laser pulse, which creates population in the excited state and leaves a hole in the ground state. Both will relax toward equilibrium, which involves a shift of their central energy and a broadening.

a relatively small Stokes shift, lies in the broadening of the bands (Figure 6 and Figure 7).

In our experiment we pump the red side of the absorption band (Figure 2), to avoid excess vibrational excitation in the excited state. Thus intramolecular vibrational relaxation processes, previously observed upon 500 nm excitation,<sup>35</sup> play a minor role, and the dynamics measured in our transient spectra predominantly reflect pure solvation dynamics resulting from the solvent response. Other intramolecular decay channels, such as, e.g., singlet—triplet conversion, occur on a much slower nanosecond time scale<sup>61</sup> and are not considered here.

In our transient spectra we have positive signals resulting from excited-state absorption of eosin Y, whose maximum is around 420 nm,<sup>57</sup> or from the dye oxidized state.<sup>35</sup> Since it appears at the spectral limit of our white-light continuum, we cannot really quantify and analyze this part, but it is clear that the excited-state absorption band overlaps at least with parts of the blue side of the absorption band and complicates the analysis of the subtle dynamics in this range.

To relate our experimental data to underlying microscopic solvation dynamics we describe the pump—probe experiment using the doorway-window picture. See Assuming the inhomogeneous limit with slow relaxation, simple analytic expressions can describe the transient absorption signal including broadening and shifts. For the case of static broadening, the absorption and fluorescence line shapes  $\sigma_a$ ,  $\sigma_f$  are Gaussians. We included a vibronic progression to phenomenologically account for the shoulder in the static spectra.

$$\sigma_{\rm a}(\omega) = \frac{1}{\sqrt{2\pi\Delta_j^2}} \sum_{n} |\mu_{\rm ng}|^2 \exp\left(-\frac{(\omega - \omega_{\rm eg}^0 - n\omega_{\rm vib} - \lambda_j)^2}{2\Delta_j^2}\right) (5)$$

$$\sigma_{\rm f}(\omega) = \frac{1}{\sqrt{2\pi\Delta_{\rm j}^2}} \sum_{n} |\mu_{\rm en}|^2 \exp\left(-\frac{(\omega - \omega_{\rm eg}^0 + n\omega_{\rm vib} + \lambda_{\rm j})^2}{2\Delta_{\rm j}^2}\right) (6)$$

 $\Delta_j$  is the inhomogeneous broadening,  $\omega_{\rm eg}^{\ 0}$  is the transition energy,  $\omega_{\rm vib}$  the vibrational spacing,  $\lambda_i$  the displacement (half

the Stokes shift),  $\mu_{ng}$  the transition dipole moment between the ground state and the vibronic state n of the electronically excited state, and  $\mu_{\rm en}$  the transition dipole moment between the lowest level in the electronically excited state and the nth vibrational level of the ground state. In the static limit of line broadening, it is possible to go beyond the snapshot limit and calculate the spectrum for pulses that are short compared with nuclear dynamics. Assuming Gaussian profiles with width  $w_i$  for pump and probe pulses, one finally can obtain an analytical expression for the pump-probe signal.<sup>58</sup>

$$\begin{split} S_{\rm pp}(\omega_1, \omega_2; \tau) & \propto \left[ (\Delta_j^2 + w_1^2) \alpha(\tau)^2 \right]^{-1/2} \sum_n \\ & \exp \left[ -\frac{(\omega_1 - \omega_{\rm eg}^0 - \lambda_j)^2}{2(\Delta_j^2 + w_1^2)} \right] \left\{ \left| \mu_{\rm ng} \right|^2 \exp \left[ -\frac{(\omega_2 - \omega_{\rm e}(\tau))^2}{2\alpha(\tau)^2} \right] + \right. \\ & \left. \left| \mu_{\rm en} \right|^2 \exp \left[ -\frac{(\omega_2 - \omega_{\rm g}(\tau))^2}{2\alpha(\tau)^2} \right] \right\} \end{split} \tag{7}$$

with

$$\omega_{\text{e,g}}(\tau) \equiv \omega_{\text{eg}}^{0} \mp n\omega_{\text{vib}} \mp \lambda_{j} + M_{j}(\tau)(\omega_{0} - \omega_{\text{eg}}^{0} \pm \lambda_{j})$$

$$\omega_{0} \equiv \omega_{1} \frac{\Delta_{j}^{2}}{\Delta_{i}^{2} + w_{1}^{2}} + (\omega_{\text{eg}}^{0} + \lambda_{j}) \frac{w_{1}^{2}}{\Delta_{i}^{2} + w_{1}^{2}}$$

and

$$\alpha(\tau)^2 \equiv \Delta_j^2 \left[ 1 - \frac{{\Delta_j}^2}{{\Delta_j}^2 + {w_1}^2} M_j^2(\tau) \right] + w_2^2$$

M(t) is the energy gap correlation function introduced in section

The terms in the braces represent the particle and hole dynamics, which are Gaussians centered at  $\omega_{\rm e}(\tau)$  and  $\omega_{\rm g}(\tau)$ , respectively. With our excitation conditions on the red edge, the particle will relax toward longer wavelength, while the relaxation of the hole will result in a blue shift of the bleach signal. Both contributions have a spectral width  $\alpha(\tau)$  which increases with time. Using eq 7, we can describe the broadening of the main band, which in fact results from two mechanisms, the blue- and red-shift of the bleach and stimulated emission components, respectively, and their broadening. If the stimulated emission is weaker than the bleach, which agrees with the results in ref 57, we find a blue shift of the maximum of the overall signal, as is the case in our experimental results.

We used the steady-state spectra to deduce values for the energy gap  $(\omega_{eg}^{0})$ , the Stokes shift (i.e., for  $\lambda$ ), and the broadening  $\Delta$ , as well as the parameters of the vibrational progression. Experimental and simulated spectra are compared in Figure 9 and the parameters used for the fit are listed in Table 2. For the vibronic progression we assumed a Poisson-like distribution  $|\mu_{\rm en}|^2 = \sigma |\mu_{\rm ng}|^2 \propto (S^n/n!)$  with a "Huang Rhys factor" of S = 0.4 and a ratio between stimulated emission and absorption  $\sigma$ .

Note that this approximation by no means represents a comprehensive description of the electronic and vibrational structure, underlying the absorption spectrum. While the assumption of only a single relevant excited electronic state should be sufficient, there are many intramolecular modes that contribute to the spectrum.8 Assuming only a single harmonic vibrational mode is a rather crude approximation, which

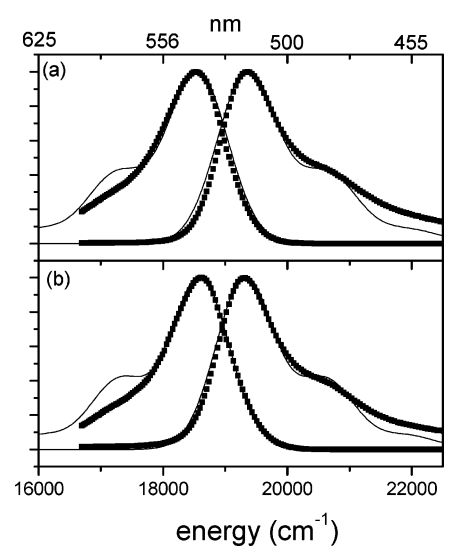


Figure 9. Experimental and calculated (eq 5, eq 6) absorption and fluorescence spectrum of (a) eosin and (b) eosin at the surface of ZrO<sub>2</sub>.

TABLE 2: Parameters for the Simulation of the Steady-State Absorption and Emission Lineshapes (See Text and Figure 9)

	water	$ZrO_2$
laser excitation-WL ( $\omega_L$ )	18690 cm <sup>-1</sup>	18690 cm <sup>-1</sup>
laser width (fwhm)	$1400 \text{ cm}^{-1}$	$1400 \ {\rm cm^{-1}}$
electronic E-gap $(\omega_e^0)$	18957 cm <sup>-1</sup>	$18957 \text{ cm}^{-1}$
Stokes Shift/2 (λ)	$400 \text{ cm}^{-1}$	360 cm <sup>-1</sup>
vibrational spating ( $\omega_{\rm wib}$ )	$1300 \text{ cm}^{-1}$	$1300 \text{ cm}^{-1}$
Huang $-$ Rhys factor ( $S_i$ )	0.4	0.4
bandwidth $(\Delta)$	$480 \text{ cm}^{-1}$	$465 \text{ cm}^{-1}$
M(t) times	2.5 fs, 700 fs, 6.6 ps	2.5 fs, 700 fs, 12 ps, ∞
M(t) prefactors	0.55, 0.15, 0.30	0.65, 0.15, 0.08, 0.13
σ	0.7	0.7

nevertheless appears sufficient for our primary goal of a phenomenological description and a qualitative understanding of the signal.

Parts b and d of Figure 6 show the time-resolved spectra that were calculated using eq 7, with the decay times obtained from the PEPS measurements for M(t). Even though there are the same inaccuracies (e.g., the shoulders in Figure 6 and Figure 9) due to the simplicity of the model, we nicely reproduce the qualitative features, especially the blue shift of the peak maximum and the broadening, and in particular the fact that it is more pronounced for eosin in water. Note that a pronounced ultrafast initial decay was necessary to correctly reproduce the initial experimental data, indicating ultrafast homogeneous broadening beyond our temporal resolution. Furthermore, the residual constant part in M(t) for eosin at  $ZrO_2$ , as retrieved from the PEPS signal, is responsible for the strongly reduced broadening effect compared to bulk water.

From the nonvanishing residual peak shift, we deduce the static broadening, which we think can be attributed to different binding sites and adsorbate conformations at the surface, which interchange on time scales slower than 100 ps. According to Cho et al.<sup>63</sup> the photon echo peak shift at infinite delay times can be estimated to be

$$\tau(\infty) = \frac{\hbar \Delta^2 \sqrt{\Gamma + \Delta^2 + \lambda^2}}{\sqrt{\pi} (\Gamma(\Gamma + 2\Delta^2 + \lambda^2) + \Delta^2 \lambda^2)}.$$
 (8)

 $\Delta$  is the inhomogeneous broadening.  $\lambda$  is the reorganization energy and  $\Gamma = 2 \lambda/\beta$ , where  $\beta = 1/kT$ . For a residual peak

TABLE 3: Result of Biexponential Fits of the Bandwidth Correlation Function (W(t), See Figure 7b) of Eosin in Water and at the Surface of  $ZrO_2$ 

	$A_1$	$t_1$	$A_2$	$t_2$	$y_0$
water	$0.30 \pm 0.03$	$210 \pm 60$	$0.72 \pm 0.03$	$6300 \pm 700$	$0.02 \pm 0.01$
water/ZrO <sub>2</sub>	$0.31 \pm 0.04$	$295 \pm 50$	$0.73 \pm 0.03$	$10200 \pm 1200$	$-0.02 \pm 0.01$

shift of ca. 2 fs and  $\lambda = 360 \text{ cm}^{-1}$ , we would estimate an inhomogeneous broadening of ca. 300 cm<sup>-1</sup>.

Another unbiased way to extract quantitative information of the broadening directly from the experiments without using mathematical model assumptions is to estimate the width of the main transient signal by calculating the variance  $(\sigma(\tau)^2)$ , i.e., the second moment of the signal in the region from 487 to 574 nm, which is plotted in Figure 7a for eosin in water and for adsorbed eosin. Note that within our simple model the increase of the spectral width with time is directly given by  $\alpha(t)$  in combination with the shift of the ground-state bleaching and stimulated emission band and should follow the correlation function M(t), which, as outlined in section II is directly proportional to the solvation function. The initial signals at  $\tau$ = 0 in bulk water and at the surface have about the same width, but the final broadening in water is much larger than that at the interface. To compare the dynamics, we calculated the bandwidth correlation function W(t) (eq 3), which is shown in Figure 7b. We obtain similar results as from the PEPS decays. The decays observed are biexponential with decay times in the region of 300 fs and 6 ps, respectively, 10 ps.

#### Discussion

The results from PEPS measurements reveal a slow decay in the range of a few picoseconds as well as subpicosecond relaxation dynamics, which is reflected by an ultrafast and a 700 fs lifetime component. From the pump—probe experiments, where the cross phase modulation at zero time delay makes analysis near t = 0 problematic, we find only one subpicosecond decay and a slower component, very similar to that of the PEPS. Both experiments confirm that the short component is unchanged for eosin in water and at the surface, while the slow dynamics becomes significantly longer at the surface. Previous fluorescence up-conversion studies have shown unchanged decay times and only differences in the preexponential factors of the two components in a biexponential fit. 29-31 However, in these measurements only subpicosecond dynamics were recorded. Also, since in these experiments it was impossible to excite at the red edge of the absorption band, intramolecular vibrational relaxation might have influenced the signals.

Solvation dynamics in water are complex and far from fully understood. Nonexponential behavior of the solvation function is known, but the assignments of different contributions are still controversial.<sup>64</sup> There are several different processes which span various time scales,<sup>2</sup> and even though we used a bi- and triexponential fit to describe our data, this should not imply separate processes, but rather is meant as a parametrization of the underlying dynamics to discuss here, following the literature, in terms of faster and slower mechanisms.

For fastest time scales the initial drop in the PEPS decays, as well as the increased width of the transient spectra in the pump—probe data at 40 fs, univocally indicates that a large part of the solvation occurs already on ultrafast time scales beyond the temporal resolution of our experiments. It is well-known that the ultrafast *inertial* contributions to solvation from small amplitude librational motions constitute the major part of the total solvation. <sup>11</sup> In our simple model, we estimated it to  $\sim$ 60% (cf. Table 2), which is close to results of coumarin 343 in water. <sup>11</sup>

High-frequency intermolecular contributions found in IR and Raman spectra of water include the librational region between 1000 and 300 cm<sup>-1</sup> and hindered translational bands below 300 cm<sup>-1</sup>. There is a strong band at about 180 cm<sup>-1</sup>, which is assigned to H-bond stretching, and restricted translation parallel to the OH-O hydrogen bond. Another weaker band at about 60 cm<sup>-1</sup> corresponds to H-bond bending or restricted translational motion perpendicular to the hydogen bond. Corresponding dynamics were also found in time-resolved experiments, including OKE, 12 TRSS, 11 and PEPS8,26 measurements, and they are representative for the collective motions of the hydrogen-bond network in water. Although intramolecular relaxation processes within the chromophore can also contribute to the signal, <sup>36</sup> for our excitation conditions on the red edge of the absorption spectrum, libration and intermolecular vibrations of the water network should play the dominant role in the initial part of solvation<sup>13</sup> and we think that these processes contribute collectively to the subpicosecond decay we observe in our experiment. Due to our temporal resolution, there are processes in the 10 fs to 1 ps range, all together parametrized in this decay, which remains the same for the case in bulk water and at the surface. We interpret this as a signature that the fast intermolecular collective dynamics of water do not change significantly close to the ZrO<sub>2</sub> surface. It seems that the properties of the hydrogen network and its high-frequency collective dynamics are not significantly influenced by the presence of the surface. Actually the probe chromophore itself already presents a strong perturbation to the water structure, and from our results it might be more correct to state only that the surface does not introduce an additional significant influence on the collective and ultrafast response of the water shells surrounding the dye. In this context the metal oxide surface behaves very different from phospholipid/water interfaces, where the absence of a  $\sim$ 1 ps solvation decay in 3PEPS experiments was explained by strong interruption of the hydrogen bond network.<sup>7</sup>

The dye binds to the  $ZrO_2$  surface via the carboxylic moiety (cf. Figure 1), and from simple geometric considerations we estimate the distance of the chromophore part from the surface to be about 5 Å. Therefore, we draw the conclusion that the effective thickness, where ultrafast water dynamics are strongly influenced by the surface, is significantly less than 5 Å, which actually is in good agreement with experimental results from up-conversion studies of dyes attached to proteins<sup>24</sup> and OKE measurements in nanopores<sup>65</sup> as well as recent theoretical estimations of aqueous  $TiO_2$  surfaces. <sup>66,67</sup>

On the other hand, the picosecond dynamics we observe get significantly slower at the surface. The assignment of this component is quite controversial in the literature. It is worth noting, that a decay time slower than 1 ps was not observed in previous time-dependent Stokes shift measurements  $^{11,24,29}$  but was seen in photon echo peak shift measurements. As outlined above, within the Debye model, our experiments should be sensitive to the *longitudinal* decay time  $\tau_L$  of the dielectric relaxation, which is faster than the Debye relaxation time. On the other hand, it is well-known that water shows a much more complex behavior and cannot adequately be described with a single Debye relaxation. Jonas and coworkers of recently found that the slowest IR144 relaxation in both acetonitrile and propylene carbonate is similar to the Debye

relaxation time, and they speculated that, from a molecular point of view (the formal positive and negative charges in IR144 are separated by ca. 8 Å, compared to solvent size of ca. 3 Å), one might argue that the charge rearrangement in IR144 is closer to a pair of macroscopic electrodes (Debye relaxation) than a point dipole (longitudinal relaxation) so that a Debye relaxation is not unreasonable.

The longest time scales in aqueous relaxation were previously attributed to relaxation of the hydrogen bond network of bulk water.<sup>70</sup> Recently, Vöhringer and co-workers<sup>1,7</sup> argued from comparison of their OKE data with NMR studies that the slow picosecond component stems from single molecule motion. On the other hand, it seems difficult to make a clear distinction between a diffusive single molecule process and collective motion in a liquid, since single molecule diffusion can be considered as the result of a molecule moving stochastically in the potential created by the other molecules and involving formation and breaking of hydrogen bonds, making it a process that inherently involves more than the single molecule under consideration.<sup>64</sup> Slowing down of diffusional motion at interfaces was indicated by recent molecular dynamics simulations, which showed a reduced diffusion coefficient in the vicinity of the TiO<sub>2</sub> surface up to a distance of 15 Å.<sup>67</sup> Commonly the longest time decay is prevalently associated with rearrangements of local structures and overall structural relaxation and recent OKE investigations found that water dynamics is characterized by a broad distribution of time scales, suggesting the presence of a large variety of relaxing structures.<sup>2</sup>

Another explanation might lie in the reduced exposure of the dye to the solvent bath due to the geometric effect of the surface. Energy exchange between the dye (and possibly its first solvent shell) with the bulk solvent can only occur to one side since half of the molecule is shielded by the surface slowing down the process. The ZrO2 surface, in this picture, influences the dynamics not by changing the properties of the water around the dye but rather by excluding half of the surrounding water molecules and thus reducing diffusive exchange and the coupling of the dye to these dynamics in the bath. This would also be a signature of the microscopic molecular properties of water and the limitation of the dielectric continuum model, where just excluding half of the solvent would not change the solvation relaxation time. This interpretation would imply very weak coupling of the molecule's modes to the surface, since the crystalline ZrO<sub>2</sub> would rather be expected to dissipate excess energy faster than the solvent. Dielectric continuum theory predicts effects from the surface due to mirror charges, which however should be minor for molecular size particles.<sup>30,71</sup> Strong modification of the dielectric constant and a much lower effective solvent polarity are expected close to the surface, which should have a direct strong influence on the longitudinal dielectric relaxation time  $\tau_L$  (see eq 4). Since we do not see a major effect on our fast decay component, it probably means that the relevant region is too narrow to be efficiently probed by our dye. We also cannot exclude contributions of specific solute-solvent interactions, which get modified by the presence of the surface. It was shown that solvation by hydrogen bonding occurs on the time scale of tens of picoseconds. 72 However, previous solvation experiments with eosin Y in water<sup>8</sup> could well be explained in terms of pure aqueous solvation and no specific influences were observed. Another influence could come from the use of buffer solutions. The ionic strength might have some influence on the solvation dynamics and it could vary close to the surface. However, these influences in the strongly polar water are expected to be small and pump-probe investigations with very high ion concentration have shown that there is not much influence of the ion strength on the hydrogen network and the local ordering in water.<sup>73</sup> Furthermore recent calculations indicate that the influence close to the TiO2 surface should be restricted to a distance of few angstroms.<sup>67</sup>

#### **Conclusions**

We performed time-resolved investigations of aqueous solvation, to compare the behavior of bulk water, with water in the proximity of metal oxide surfaces. In contrast to previous fluorescence investigations of the time-resolved Stokes shift of dyes attached to proteins<sup>25</sup> and PEPS measurements of interfacial water at membranes, our results indicate very limited influences of the surface onto the dye probe. We believe that the most probable explanation lies in the bulky size of the chromophores and that the effective interfacial water layer is very thin, extending over not much more than one monolayer and that there is very little effect of the interfacial (mono)layer on the dynamics of the following water layers. It seems that also effects from changes in the dielectric constant are restricted to this interface, too narrow to influence the probe, and we estimate a maximum interface thickness of ca. 5 Å. On the other hand, picosecond relaxation processes are affected significantly by the surface. The most probable explanation seems to be a slowdown of diffusional motions and structural relaxation, but our results cannot exclude several different scenarios, as outlined above.

For probing the dynamics of the interfacial layer, timeresolved OKE measurements of water in porous TiO2 films avoid the necessity of bulky dyes and are being carried out at present.

Acknowledgment. We thank Professor S. Steinemann for suggesting this study and for useful discussions. This work was supported by a grant from the ITI foundation for the Promotion of Implantology, Switzerland, and by the Swiss NSF via the NCCR: "Quantum Photonics" and Contracts 200020-105344, 205320-101825, and 2000-67912.02.

## **References and Notes**

- (1) Winkler, K.; Lindner, J.; Bürsing, H.; Vöhringer, P. J. Chem. Phys. 2000, 113, 4674.
  - (2) Torre, R.; Bartolini, P.; Righini, R. Nature 2004, 428, 296.
- (3) Laenen, R.; Rauscher, C.; Laubereau, A. Phys. Rev. Lett. 1998, 80. 2622.
- (4) Yeremenko, S.; Pshenichnikov, M. S.; Wiersma, D. A. Chem. Phys. Lett. 2003, 369, 107.
- (5) Stenger, J.; Madsen, D.; Hamm, P.; Nibbering, E. T. J.; Elsaesser, T. Phys. Rev. Lett. 2001, 87, 27401.
- (6) Cowan, M. L.; Bruner, B. D.; Huse, N.; Dwyer, J. R.; Chugh, B.; Nibbering, E. T. J.; Elsaesser, T.; Miller, R. J. D. Nature 2005, 434, 199.
- (7) Bürsing, H.; Ouw, D.; Kundu, S.; Vöhringer, P. Phys. Chem. Chem. Phys. 2001, 3, 2378.
- (8) Lang, M. J.; Jordanides, X. J.; Song, X.; Fleming, G. R. J. Chem. Phys. 1999, 110, 5884.
- (9) Ausbury, J. B.; Steinel, T.; Stromberg, C.; Corcelli, S. A.; Lawrence, C. P.; Skinner, J. L.; Fayer, M. D. J. Phys. Chem. A 2004, 108, 1107.
- (10) Woutersenand, S.; Bakker, H. J. Phys. Rev. Lett. 1999, 83, 2077. (11) Jarzeba, W.; Walker, G. C.; Johnson, A. E.; Kahlow, M. A.;
- (12) Jimenez, R.; Fleming, G. R.; Kumar, P. V.; Maroncelli, M. Nature **1994**, 369, 471
- (13) Pal, S. K.; Peon, J.; Bagchi, B.; Zewail, A. H. J. Phys. Chem. 1992, 106, 12376.
- (14) Du, Q.; Freysz, E.; Shen, Y. R. Phys. Rev. Lett. 1994, 72, 238.
- (15) Miranda, P. B.; Shen, Y. R. J. Phys. Chem. B 1999, 103, 3292.
- (16) Richmond, G. L. Annu. Rev. Phys. Chem. 2001, 52, 357.

Barbara, P. F. J. Phys. Chem. 1988, 92, 7039.

- (17) Shang, X.; Benderskii, A. V.; Eisenthal, K. B. J. Phys. Chem. B **2001**, 105, 11578.
- (18) Kornherr, A.; Vogtenhuber, D.; Ruckenbauer, M.; Podloucky, R.; Zifferer, G. J. Chem. Phys. 2004, 121, 3722.

- (19) Scatena, L. F.; Brown, M. G.; Richmond, G. L. Science 2001, 292, 908.
- (20) Benham, M. J.; Cook, J. C.; Li, J. C.; Ross, AD. K.; Hall, P. L.; Sarkissian, B. *Phys. Rev. B* **1989**, *39*, 633.
  - (21) Bellissent-Funel, M. C. J. Phys.: Condens. Matter 2001, 13, 9165.
- (22) Nandi, N.; Bhattacharyya, K.; Bagchi, B. Chem. Rev. 2000, 100, 2013 and references herein.
- (23) Zhong, D.; Pal, S. K.; Zhang, D.; Chan, S. I.; Zewail, A. H. *Proc. Natl. Acad. Sci. U.S.A.* **2002**, *99*, 13.
- (24) Pal, S. K.; Peon, J.; Zewail, A. H. Proc. Natl. Acad. Sci. U.S.A. 2002, 99, 1763.
- (25) Peon, J.; Pal, S. K.; Zewail, A. H. *Proc. Natl. Acad. Sci. U.S.A.* **2002**, *99*, 10964.
- (26) Bürsing, H.; Kundu, S.; Vöhringer, P. J. Phys. Chem. B 2003, 107, 2404.
- (27) Ruan, C.-Y.; Lobastov, V. A.; Vigliotti, F.; Chen, S.; Zewail, A. H. *Science* **2004**, *304*, 80.
  - (28) Grätzel, M. Nature 2001, 414, 338.
  - (29) Pantand, D.; Levinger, N. E. Chem. Phys. Lett. 1998, 292, 200.
  - (30) Pantand, D.; Levinger, N. E. J. Phys. Chem. B 1999, 103, 7846.
- (31) Tortschanoff, A.; Portuondo-Campa, E.; van Mourik, F.; Moser, J. E.; Steinemann, S.; Chergui, M. In *Femtochemistry and Femtobiology: Ultrafast Events in Molecular Science*; Martins, M., Hynes, J. T., Eds.; Elsevier Science Publishers: Amsterdam, 2004; p 541.
- (32) Martins, L. R.; Skaf, M. S.; Ladanyi, B. M. J. Phys. Chem. B 2004, 108, 19687.
- (33) Shang, X.; Benderskii, A. V.; Eisenthal, K. B. J. Phys. Chem. B **2001**, 105, 11578.
- (34) Huber, R.; Spörlein, S.; Moser, J. E.; Grätzel, M.; Wachtveitl, J. J. Phys. Chem. B 2000, 104, 8995.
  - (35) Pelet, S.; Grätzel, M.; Moser, J. E. J. Phys. Chem. 2003, 107, 3215.
- (36) Kovalenko, S. A.; Ruthmann, J.; Ernsting, N. P. Chem. Phys. Lett. 1997, 271, 40.
- (37) Chandler, D. Introduction to Statistical Mechanics; Oxford University Press: New York, 1989; Chapter 8.
- (38) Aherne, D.; Tran, V.; Schwartz, B. J. J. Phys. Chem. B 2000, 104, 5382.
- (39) Larrégaray, P.; Cavina, A.; Chergui, M. Chem. Phys. 2005, 308,
- (40) Nishiyamaand, Y.; Okada, T. J. Phys. Chem. A 1997, 101, 5729.
- (41) Nishiyama, K.; Asano, Y.; Hashimoto, N.; Okada, T. J. Mol. Liq. 1995, 65/66, 41.
  - (42) Carterand, E. A.; Hynes, J. T. J. Chem. Phys. 1991, 94, 5961.
  - (43) Strattand, R. M.; Maroncelli, M. J. Phys. Chem. 1996, 100, 12981.
- (44) Nilssonand, L.; Halle, B. Proc. Natl. Acad. Sci. U.S.A. 2005, 102, 13867.
- (45) de Boeij, W. P.; Pshenichnikov, M. S.; Wiersma, D. A. Annu. Rev. Phys. Chem. **1998**, 49, 99.

- (46) Fleming, G. R.; Joo, T.; Cho, M. Adv. Chem. Phys. 1997, 101, 141
- (47) de Boeij, W. P.; Pshenichnikov, M. S.; Wiersma, D. A. J. Phys. Chem. 1996, 100, 11806.
  - (48) Bookand, L. D.; Scherer, N. F. J. Chem. Phys. 1999, 111, 792.
- (49) van der Zwanand, G.; Hynes, J. T. *J. Phys. Chem.* **1985**, *89*, 4181; van der Zwan, G.; Hynes, J. T. *J. Chem. Phys.* **1982**, *76*, 2993.
  - (50) Friedman, H. J. Chem. Soc., Faraday Trans. 2 1983, 79, 1465.
- (51) Schenkl, S.; van Mourik, F.; van der Zwan, G.; Haacke, S.; Chergui, M. Science 2005, 309, 917.
  - (52) Moserand, J.; Grätzel, M. J. Am. Chem. Soc. 1984, 106, 6557.
- (53) Chuangand, T. J.; Eisenthal, K. B. Chem. Phys. Lett. 1971, 11, 368.
- (54) Fleming, G. R.; Morris, J. M.; Robinson, G. W. Chem. Phys. 1976, 17, 1991.
- (55) Lakowicz, J. R. *Principle of Fluorescence Spectroscopy*, 2nd ed.; Kluwer Academic/Plenum Publishers: New York, 1999.
  - (56) Thompson, W. H. J. Chem. Phys. 2004, 120, 8125.
- (57) Penzkofer, A.; Beidoun, A.; Speiser, S. Chem. Phys. 1993, 170, 139.
- (58) Mukamel, S. *Principles of Nonlinear Optical Spectroscopy*; Oxford University Press: New York, 1995.
  - (59) Kinoshita, S. J. Chem. Phys. 1989, 91, 5175.
  - (60) Yu, J.; Kang, T. J.; Berg, M. J. Chem. Phys. 1991, 94, 5787.
  - (61) Penzkofer, A.; Beidoun, A.; Daiber, M. J. Lumin. 1992, 51, 297.
- (62) Loring, R. F.; Yan, Y. J.; Mukamel, S. J. Chem. Phys. 1987, 87, 5840.
- (63) Cho, M.; Yu, J.-Y.; Joo, T.; Nagasawa, Y.; Passino, S. A.; Fleming, G. R. J. Phys. Chem. 1996, 100, 11944.
  - (64) Rønne, C.; Keiding, S. R. J. Mol. Liq. 2002, 101, 199.
  - (65) Scodinu, A.; Fourkas, J. T. J. Phys. Chem. B 2002, 106, 10292.
- (66) Opitz, A.; Ahmed, S. I.-U.; Schaefer, J. A.; Scherge, M. Surf. Sci. 2002, 504, 199.
- (67) Predota, M.; Bandura, A. V.; Cummings, P. T.; Kubicki, J. D.; Wesolowski, D. J.; Chialvo, A. A.; Machesky, M. L. *J. Phys. Chem. B* **2004**, *108*, 12049.
- (68) Buchner, R.; Barthel, J.; Stauber, J. Chem. Phys. Lett. 1999, 306,
- (69) Yu, A.; Tolbert, C. A.; Farrow, D. A.; Jonas, D. M. J. Phys. Chem. A 2002, 106, 9407.
- (70) Baar, Ch.; Buchner, R.; Kunz, W. J. Phys. Chem. B 2001, 105, 2906.
  - (71) van der Zwanand, G.; Mazo, R. M. J. Chem. Phys. 1985, 82, 3344.
  - (72) Yuand, J.; Berg, M. Chem. Phys. Lett. 1993, 208, 315.
- (73) Willem Omta, A.; Kropman, M. F.; Woutersen, S.; Bakker, H. J. *Science* **2003**, *301*, 347. Willem Omta, A.; Kropman, M. F.; Woutersen, S.; Bakker, H. J. *J. Chem. Phys.* **2003**, *119*, 12457.